Near field characterization of the GeoSTAR demonstrator

A. B. Tanner, B. H. Lambrigsten, T. M. Gaier
Jet Propulsion Laboratory
California Institute of Technology
Pasadena, USA
alan.b.tanner@jpl.nasa.gov

F. Torres[1]
Department of Signal Theory and Communications
Polytechnic University of Catalonia
Barcelona, Spain
xtorres@tsc.upc.edu

***Abstract*— The GeoSTAR demonstrator can be characterized at close range by means of a simple near-to-far-field phase correction. This reduces the test set-up configuration to reasonable dimensions. In order to simulate the Earth as seen from GEO, the target consists of a disc of absorbent material at ambient temperature placed against the sky. This work presents the details of the near-to-far-field correction as well as some preliminary results that confirm its suitability to characterize the demonstrator.**

Keywords-remote sensing; radiometer; interferometer; near field.

I. INTRODUCTION

GeoSTAR represents a new approach to microwave atmospheric sounding from geostationary orbit based on passive interferometry [1]. This new instrument will eventually be deployed in geostationary orbit to complement future infrared sounders and enable allweather temperature and humidity soundings and rain mapping. In order to achieve a spatial resolution of 50 km, about 300 receiving units, arranged in a Y shape configuration, are required to compound a 2-D interferometric system. Cross-correlations between the output signals give a symmetric hexagonal sampling grid of the so-called visibility function in the u-v space (antenna separation measured in wavelengths). Fourier-like techniques are then used to retrieve the brightness temperature map from these visibility samples. GeoSTAR unambiguous field of view (UFoV), which is given by the minimum separation between antennas, is set to about 17.5 deg in order to sustain the Earth disc as seen from GEO.

The Jet Propulsion Laboratory is currently leading the development of a low-resolution (1 deg) ground prototype consisting of 24 receiving units in the same configuration than the GEO instrument [2] -fig. 1-. This gives and image with 385 independent pixels or about 17 pixels for a horizontal cut. In order to assess the imaging capabilities of the instrument, a calibration target has been designed to emulate/reproduce the Earth view as seen from GEO. It consists of a disk, made of absorbent material, placed against the cold sky background. Some heaters are properly distributed to give temperature contrast. Several sensors give continuous temperature readings of the target. Far Field (FF) characterization of the instrument would require the target to be placed close to 100 m. In this case, in order to fill the UFoV, a target diameter of about 30 m would be required. Instead, a Near Field (NF) characterization at 10 m is foreseen so as to constrain target diameter size to 3 m and ease temperature control and monitoring.

NF measurements require some kind of correction since the approximations underlying conventional FF interferometric imaging are no longer valid. In [3] the antennas are arranged in an out-of-plane circular array so as to create an equivalent FF volume close to its center. In [4], NF images are obtained by

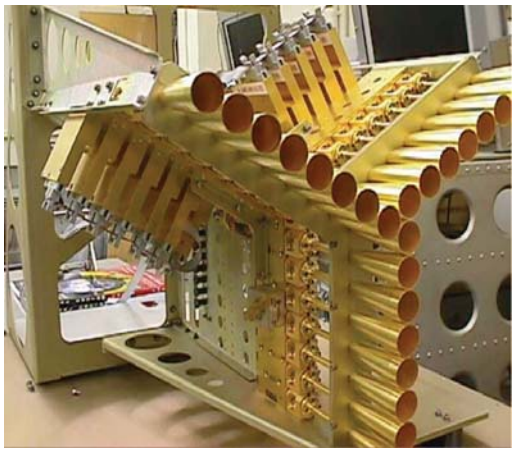

Figure 1. GeoSTAR demonstrator [2].

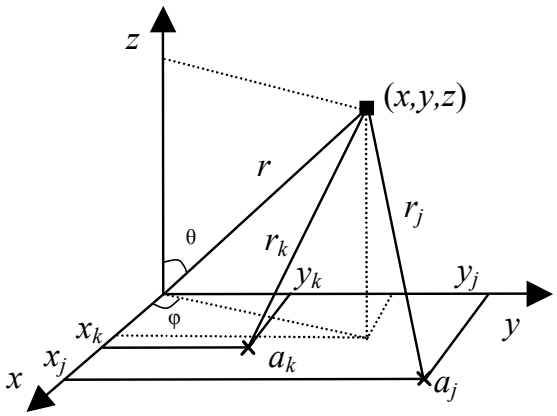

Figure 2. Near field geometry for two antennas a_k and a_j in the observation plane XY and a pixel placed at (x,y,z).

This work has been carried out at the Jet Propulsion Laboratory, California Institute of Technology under a contract with the National Aeronautics and Space Administration.

[1]F. Torres currently on sabbatical leave at the JPL, CalTech, under grant PR2005-0427, Spanish Ministry of Education & Science.

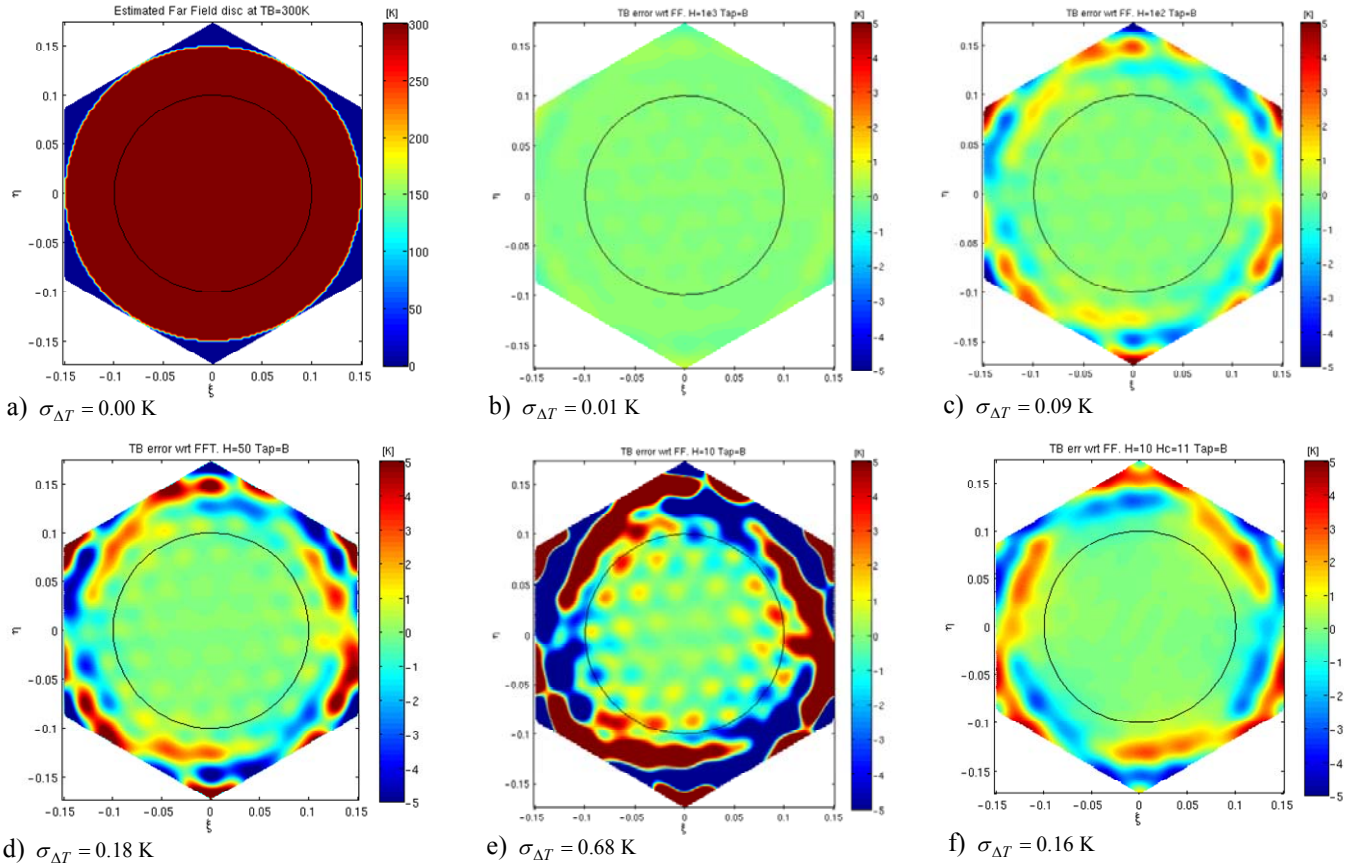

a) $\sigma_{\Delta T} = 0.00$ K b) $\sigma_{\Delta T} = 0.01$ K c) $\sigma_{\Delta T} = 0.09$ K

d) $\sigma_{\Delta T} = 0.18$ K e) $\sigma_{\Delta T} = 0.68$ K f) $\sigma_{\Delta T} = 0.16$ K

Figure 3. **a)** Target as measured in FF by an ideal instrument (300 elements). **b)**, **c)**, **d)** and **e)** difference between FF and NF images measured by the demonstrator (24 elements) for targets at H=1000, 100, 50 and 10 m. Error computed within the circle r=0.1, which is the 45º incidence angle on Earth form GEO. **f)** Difference between NF and FF for a target at H=10 m after applying NF phase correction with H_c=11m.

inverting the NF equations. In [5] it is shown that a single pixel in the UFoV can be focused by correcting the NF phase error. In the present work, this last technique will be used to show that a simple phase correction mask, applied to the NF visibility samples, completely focuses the pixel placed at boresight whereas it produces a smooth defocusing errors for pixels off-boresight. After NF correction, far field image retrieval tools can be used without any additional modification.

II. NEAR FIELD VISIBILITY

Taking into account a flat temperature distribution placed at a height z, the near field (NF) visibility in Kelvin measured by two antennas a_k and a_j, placed in the XY plane (fig. 2) can be written as

$$V_{kj}^{NF} = \iint_{4\pi} T_B(\theta,\phi) \frac{F_{nk}(\theta_k,\phi_k) F_{nj}^*(\theta_j,\phi_j)}{\sqrt{\Omega_k \Omega_j}} \frac{r^2}{r_k r_j} e^{jk_0(r_k - r_j)} d\Omega \qquad (1)$$

where T_B is the image brightness temperature, $F_{nk,j}$ are the normalized antenna patterns –which see the image from their own coordinate system-, and $\Omega_{k,j}$ their antenna equivalent solid angles. The fringe-washing term has been neglected. The distance $r_{k,j}$ of the antennas to each pixel $T_B(\theta,\varphi)$ can be written as a function of the direction cosines (ξ=sinθcosφ, η=sinθsinφ), pixel distance r and antenna position ($x_{k,j}$, $y_{k,j}$) as:

$$r_{k,j} = r\sqrt{1 + \left(\frac{x_{k,j}}{r}\right)^2 + \left(\frac{y_{k,j}}{r}\right)^2 - \frac{2}{r}\left(x_{k,j}\xi + y_{k,j}\eta\right)} \qquad (2)$$

This expression leads to the well known FF visibility when the image is at a large distance in comparison with the array dimensions ($r >> x_{k,j}, y_{k,j}$):

$$V_{kj}^{FF} = \iint_{\xi^2+\eta^2 \le 1} \frac{T_B(\xi,\eta) F_{nk}(\xi,\eta) F_{nj}^*(\xi,\eta)}{\sqrt{1-\xi^2-\eta^2}\sqrt{\Omega_k \Omega_j}} e^{-j2\pi(\xi u_{kj} + \eta v_{kj})} d\xi d\eta \qquad (3)$$

where $u_{kj}=(x_k-x_j)/\lambda$ and $v_{kj}=(y_k-y_j)/\lambda$ are the antenna separation in wavelengths.

A. Near field distortion in the GeoSTAR prototype

The largest non-paraxial error due to NF measurements occurs for the largest baselines. The GeoSTAR prototype is a Y-shaped array with antenna separation d=22.5 mm. The antenna at the edge of the arms is placed at a distance from the array center d_{max}=18 cm, which gives an angle θ=1 deg for a pixel placed at boresight at z=10 m. This yields a maximum antenna pattern amplitude errors of $|\Delta Fn|$=0.33% for a pixel at boresight and slightly larger at the edge of the UFoV due to the antenna pattern decay. Antenna pattern phase errors and amplitude errors due to the free space propagation are negligible.

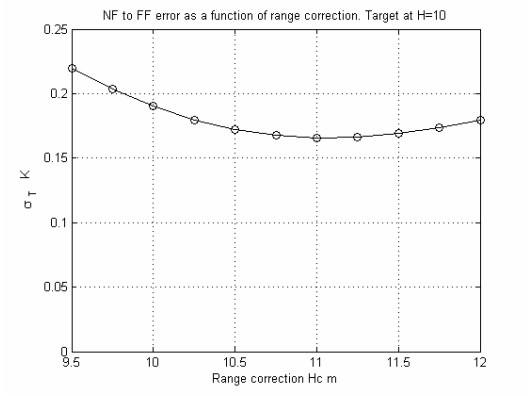

Figure 4. Sensitivity to range errors of Near Field correction. NF distortion is minimized by focusing a pixel placed at boresight at a distance slightly larger than the target range H=10 m.

However, the phase error due to differential path delay is about 70 deg for a pixel placed at boresight and, beyond z=10 m, makes NF distortion clearly dominated by these errors.

In order to analyze the impact of NF distortion some simulations are performed. The target consists of a disc at T_B=300K of radius r=0.15 in the (ξ,η) domain, which is the size of the Earth as seen from GEO. The sky background is at T_{sky}=2.7 K. Fig. 3 (a) shows the target as would be measured in FF by an ideal instrument with 300 elements. The image is constrained to the hexagonal cell given by the unambiguous field of view set by the antenna separation $d = 3.825\lambda$. The rest of plots in fig. 3 are related to the demonstrator (24 elements). Fig. 3 (b), (c), (d) and (e) show the difference in K between the estimated images in NF at H=1000, 100, 50 and 10 m and the equivalent FF image. NF visibilities are estimated according to (1) and FF visibilities according to (3). Once the visibilities are computed, an estimate of the image is retrieved by means of a rectangular iFFT over the hexagonal grid, according to the procedure given in [6]. The rms difference between NF and FF images is computed within a circle of radius r=0.1, which is the 45º incidence angle from GEO. In order to deal with the truncated spectrum of the visibility samples, a Blackman taper is used to smooth the ripple at the disc-sky border. The simulations clearly show that, in order to neglect NF distortion, the target must be placed at a distance close to 100 m. This requires a disc of absorbent material with about 15 m radius.

III. NEAR-TO-FAR-FIELD CORRECTION

In the case that only path delay phase errors are taken into account the visibility samples measured by any pair of antennas can be approximated by:

$$V_{kj}^{NF} \cong \iint_{4\pi} T_B(\theta,\phi)\frac{\left|F_{nk}(\theta,\phi)\right|^2}{\sqrt{\Omega_k\Omega_j}} e^{jk_0(r_k-r_j)}\sin\theta\, d\theta\, d\phi \qquad (4)$$

where all antennas are assumed to have the same antenna pattern. For an extended source, NF distortion can only be corrected by inverting (1). However, if we take into account a single punctual source (placed beyond 10 m) the vectors $r_{k,j}$ are well defined for all antenna pairs and it is possible to correct the NF measurements simply by subtracting the NF phase and adding the FF phase from the measurements:

$$\hat{V}_{kj}^{FF} = V_{kj}^{NF} e^{-jk_0(r_k-r_j)} e^{-j2\pi(u\xi+v\eta)} \qquad (5)$$

This correction factor has a quite smooth variation for pixels within the UFoV. This suggests that NF visibilities from an extended source can be partially corrected just by focusing the NF visibilities to the pixel at boresight. Moreover, the NF correction presents a quite low sensitivity to range errors. Fig. 4 shows the NF error wrt FF for a target placed at H=10 m, when the correction is applied for a pixel placed at boresight at distances ranging from 9.5 to 12 m. As shown, the minimum error is produced when the correction is applied at H_c=11 m. Fig. 3 (e) shows the difference between FF and NF for a target at H=10 m after applying the NF correction at H_c=11 m. The error within the area of interest (r < 0.1) is reduced to σ_T=0.16K. Some error appears at the disc-sky border due to residual antenna pattern amplitude error at the edge of the UFoV.

At H=10 m the radius of the disc is r=1.5 m, which significantly reduces the test set-up construction. Some heaters will be properly distributed and monitored within the disc. This will give a temperature contrast within the disc to better simulate a scene, as seen from GEO, and allow the test of the image retrieval procedures.

IV. PRELIMINARY RESULTS

GeoSTAR NF imaging capability has already been proved by some indoor measurements. Figure 5 (a) shows system response to a point source placed at boresight, at close range inside the laboratory (4 m), when FF inverting algorithms are applied without any kind of NF correction. The instrument phase calibration is based on previous antenna range measurements, which proved to be accurate and stable enough to produce quite good outdoors FF images [2]. As shown in fig. 5 (a), the NF image distortion clearly follows single element geometric configuratio (Y-shape). According to (5), the NF point source image can be focused simply by zeroing the NF visibility phases, which also calibrates any residual instrumental phases. Fig 5 (b) shows point source response after NF to FF correction. The point source has been centered and its FF hexagonally distributed secondary lobes are clearly seen. The NF correction used to correct the point source response is now applied to focus the image of an individual standing in front of the instrument at approximately the same range. Inside the laboratory absolute amplitude calibration was not available since the point source was not calibrated and multiple alias from the warm laboratory background –although highly attenuated by antenna pattern decay- give a significant contribution to the image. However, the warm shape of the subject in front of the colder laboratory background is clearly seen. The hot coffee pot being held by the individual is also clearly discriminated.

This results encourages the realization of the outdoor NF experiment, where the sky-alias can be well eliminated and the test set-up configuration, at the JPL external antenna range, much better controlled .

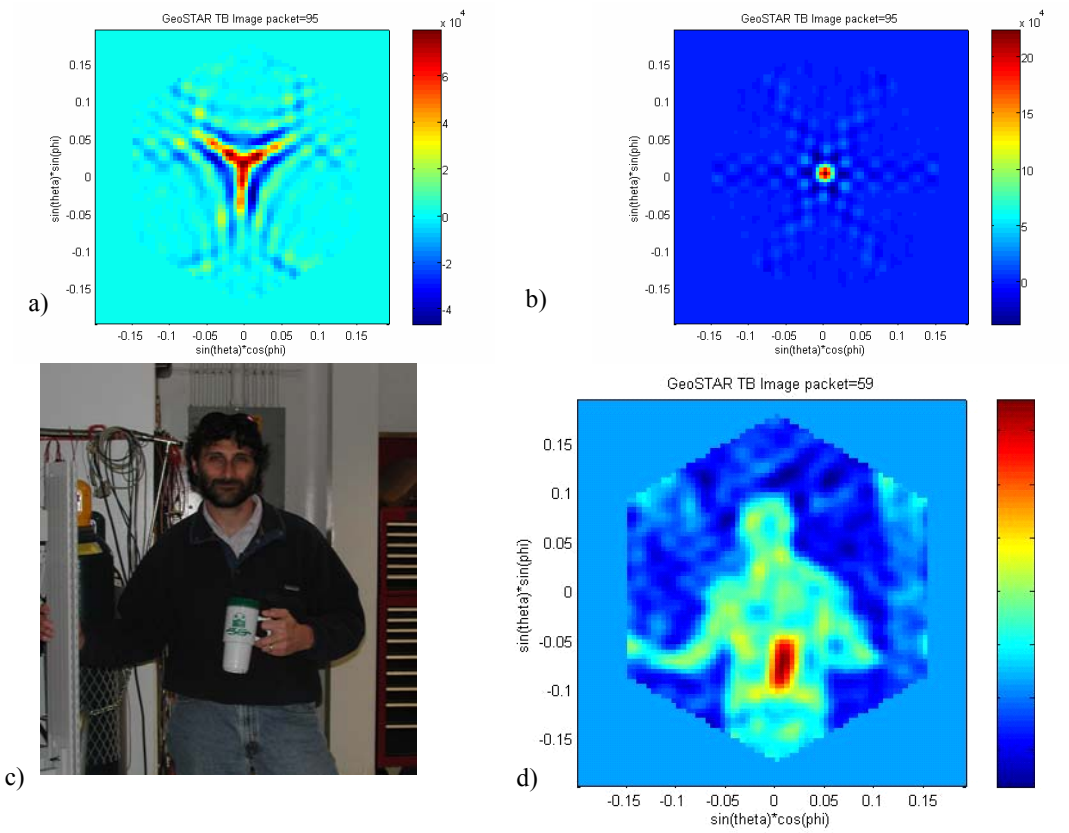

Figure 5. **a)** NF point source response without correction. **b)** Point source response after NF to FF correction. **c)** Subject standing in front of the instrument at the same range that the point source. **d)** Image of the individual after NF phase correction: the warm shape of the subject in front of the colder laboratory background and the hot coffee pot are clearly discriminated.

V. CONCLUSIONS

This presentation has shown the viability to characterize the GeoSTAR demonstrator at close range (10 m) by applying a phase mask to the measured visibility samples. The near field test highly simplifies the design and control of the measurement set-up. In order to simulate the Earth as seen from GEO, the target will consist of a disc (r=1.5 m) made of absorbent material at ambient temperature and placed against the sky background. It has been shown that near field rms distortion is constrained to 0.16 K in a large area inside the unambiguous field of view. Some heaters will be properly placed in the target to give a temperature contrast within the disc to better simulate a scene as seen from GEO and test the image retrieval procedures. Some preliminary indoor experiments have confirmed the suitability of near field test to characterize the demonstrator

ACKNOWLEDGMENT

This work has been carried out at the Jet Propulsion Laboratory, California Institute of Technology under a contract with the National Aeronautics and Space Administration.

REFERENCES

[1] B. Lambrigtsen, W. Wilson, A. Tanner, T. Gaier, C. Ruf, J. Piepmeier, "GeoSTAR - a microwave sounder for geostationary satellites". Geoscience and Remote Sensing Symposium IGARSS '04. Proceedings. 2004 IEEE International. Vol. 2, pp. 777 – 780, 2004.

[2] A. B. Tanner, S. T. Brown, S. J. Dinardo, T. M. Gaier, P. P. Kangaslahti, B. H. Lambrigtsen, W. J. Wilson, J. R. Piepmeier, C. S. Ruf, S. M. Gross, B. H., Lim, S. Musko, S. Rogacki, "Initial results of the GeoSTAR Prototype (Geosynchronous Synthetic Thinned Array Radiometer)", IEEE Aerospace Conference. Big Sky, MT USA 4-11 March 2006.

[3] B. Laursen, N. Skou, "Synthetic aperture radiometry evaluated by a two-channel demonstration model", IEEE Transactions on Geoscience and Remote Sensing, Vol. 36, N. 3, pp. 822 - 832 May 1998.

[4] M. Peichel, H. Suess, M. Suess, "Microwave imaging of the brigthness temperature distribution of extended areas in the near and far field using two-dimensional aperture synthesis with high spatial resolution", Radio Science, Vol. 33, N. 3 pp. 781-801 May-June 1998.

[5] N. Duffo, I. Corbella, F. Torres, A. Camps, M. Vall-llossera, "Advantages and drawbacks of near-field characterization of large aperture radiometers". Microrad 2004. Rome, Italy.

[6] A. Camps, J. Bara, I. Corbella, F. Torres, "The processing of hexagonally sampled signals with standard rectangular techniques: Application to 2-D large aperture synthesis interferometric radiometers". IEEE Transactions on Geoscience and Remote Sensing. Vol. 35 N. 1 pp. 183-190, Jan 1997.